International Journal of Nanoelectronics and Materials
IJNeaM
ISSN 1985-5761 | E-ISSN 2232-1535

Graphene-enhanced surface plasmon resonance in photonic crystal fiber for sensing glucose in serum

Malik J. Abd-ALhussain [a] *, Makram A. Fakhri [b] *, and Bassam G. Rasheed [a]

[a]*Al-Nahrain University, College of Engineering, Laser and Optoelectronics Engineering, Iraq*
[b]*Laser and Optoelectronic Department, University of technology-Iraq, Baghdad, Iraq*
∗Corresponding author. E-mail: mokaram_76@yahoo.com & makram.a.fakhri@uotechnology.edu.iq

Received 22 September 2023, Revised 29 March 2024, Accepted 24 July 2024

ABSTRACT

This study presents a solid-core photonic crystal fibre (PCF) with a metallic nanolayer of gold (Au)/silver (Ag) and graphene on the outer surface for glucose sensing applications. Graphene nanoparticles were prepared by pulsed laser ablation in liquid (PLAL) and then mixed with a polyvinyl alcohol (PVA) solution to coat the PCF surface. Glucose solutions with a refractive index (RI) ranging from 1.3475 to 1.3502 were used for evaluation. Results exhibit that the PCF sensor's sensitivity is significantly improved by incorporating a graphene layer onto the Au/Ag nanofilm coatings. The maximum sensitivity achieved for glucose detection in blood was 4284.243 nm/RIU and 3775 nm/RIU, with corresponding resolutions of 1×10^{-5} and 1.5×10^{-5} for graphene on Au and Ag, respectively. Experimental values yielded sensitivities of 1314 nm/RIU and 1119 nm/RIU, with resolutions of 2.5×10^{-5} and 2.7×10^{-5} for graphene on Au and Ag, respectively. Nanomaterials were investigated using a multi-technique approach encompassing transmission electron microscopy (TEM), Fourier-transform infrared spectroscopy (FTIR), Raman spectroscopy, and UV-VIS spectroscopy. TEM provided nanoscale visualization, revealing size, shape, and distribution characteristics. FTIR spectroscopy identified functional groups and bonding features, sp^2 C-C bond stretching between 1580 and 1450 cm^{-1}. Raman spectroscopy assessed structural integrity via D and G bands at 1350 cm^{-1} and 1590 cm^{-1}. UV-vis spectroscopy elucidated optical properties. Integrating metallic Au/Ag and graphene layers on the PCF exterior shows excellent potential for developing susceptible bio-chemical detection devices.

Keywords: *Photonic crystal fibre, Graphene, Gold nanolayer, Surface plasmon resonance, Sensor*

1. INTRODUCTION

In comparison to conventional fibre, the Surface Plasmon Resonance (SPR) refractive index sensor based on photonic crystal fibre (PCF) has gained a lot of research attention owing to its significant scientific applicability in the area of biological sample detection [1-3]. Surface Plasmon Resonance (SPR) is a highly sensitive optical phenomenon that occurs when light interacts with a thin metal film, typically gold (Au) or silver (Ag), and an adjacent medium, such as a liquid or a gas. This phenomenon has extensive applications in various fields, including biosensing, chemical sensing, and environmental monitoring [4-6] . The working principle of an SPR-PCF sensor involves the excitation of surface plasmons within the PCF structure through the interaction of incident light with the metal nanofilm [7-9]. When the PCF sensor is in contact with the analyte, such as a liquid sample, changes in the analyte's refractive index induce changes in the SPR response. These changes are then measured and analysed to obtain information about the analyte [10-12].

The refractive index of silica is calculated using the Sellmeier Equation (1) [13-15]:

$$n_s = \sqrt{1 + \frac{A_1\lambda^2}{\lambda - B_1^2} + \frac{A_2\lambda^2}{\lambda - B_2^2} + \frac{A_3\lambda^2}{\lambda - B_3^2}} \quad (1)$$

A_1, A_2, A_3, B_1, B_2, and B_3 are the Sellmeier constants mentioned in references [16, 17]. Drude-Lorentz model was employed for material dispersion of Au as shown below in Equation (2) [18-20]:

$$\varepsilon_m = \varepsilon_\infty - \frac{\omega_D^2}{\omega(\omega + i\gamma D)} + \frac{\Delta_\varepsilon \Omega_L^2}{(\omega^2 - \Omega_L^2) - i\Gamma_{L\omega}} \quad (2)$$

where ε_∞=5.967 is the permittivity of at high frequency and Δ_ε=1.09 is a weighting factor. ω_D is the plasma frequency, and γ_D is the damping frequency, where $\omega_D/2\pi$= 2.113 THz, $\gamma_D/2\pi$=15.92 THz, ω is the angular frequency of transmitting light, Ω_L and Γ_L represent the frequency and the spectral width of the Lorentz oscillator, respectively. Furthermore, $\Omega_L/2\pi$=650.07 THz, and $\Gamma L/2\pi$=104.86 Hz.

The complex refractive index of graphene is determined from Equation (3) [1]:

$$n_g = 3 + iS_1\frac{\lambda}{3} \quad (3)$$

where λ is the vacuum wavelength in μm and constant $S_1 \approx 5.446$ μm^{-1} [2].

This work aims to design and implement nanolayer PCF vitalizing the surface plasmon resonance for biological and biochemical sensing applications.

2. THE EXPERIMENTAL WORKS

2.1. Preparation of Graphene PVA

Graphene nanoparticles were obtained using Pulsed Laser Ablation in Liquid (PLAL) of a graphite sheet submerged in 10 mL distilled water. Before ablation, the sheet and containers were cleaned with ultrasonic cleaning in distilled water. A Q-switched Nd: YAG laser (model FQ015-1) operating at 1064 nm, with a 7 ns pulse width and 5 Hz repetition rate, was employed to irradiate the graphite target vertically. The graphene nanolayer was produced with 800 mJ laser pulses. Various characterization techniques were used for the graphene nanolayer. These include TEM, FTIR Raman, and UV-Vis absorption. The graphene-PVA solution was prepared when 1 g of PVA powder dissolved in 100 ml of deionized water (DI) at 70°C for 20 minutes. Subsequently, 10 ml of graphene solution was added to 10 ml of PVA 10 ml of PVA solution and stirred slowly for 1 hour to achieve a clear, uniform solution. Ultrasonication was then performed to disperse graphene in the PVA solution. The resulting solution was immediately used to coat the PCF, which was previously coated with a gold/silver nanolayer using the sputtering method. The PCF was dipped into the prepared solution many times and left to dry at room temperature for approximately 24 hours.

2.2. PCF Sensor

We have proposed a photonic crystal fibre sensor based on the SPR phenomenon where photonic crystal fibre (ESM-12B) is used to remove the middle portion of the PCF cladding. The sensor is developed using the finite element method (FEM) in COMSOL Multiphysics. The mesh type, materials, and geometries are chosen to measure the sensor confinement loss. The core (12 µm diameter) and the cladding (125 µm diameter) are made from silica glass. The removed cladding is coated with Au or Ag NPs (50 nm thickness), and then the outer fibre surface is coated with graphene to construct the sensor and enhance its sensitivity. The fibre is immersed in glucose dissolved in the blood (1 µm thickness) at wavelength 1520 to 1560 nm and RIs ranging (from 1.3476 to 1.3502). The experimental arrangement for the proposed photonic crystal fibre sensor contains different stages; the first stage is the laser source (Model#01 Standard type) emits wavelength (1528-1565 nm) and the sensing unit which is a segment of photonics crystal fibre (ESM-12B) made by NKT Photonics has always been an endless single-mode fibre deposited with different types of nanomaterials and the last stage was the optical spectrum analyzer (BaySpec's WaveCapture® FBGA) wavelength range (from 1525 to 1590 nm) as detection unit Figure 1 shows these stages.

Figures 2 (a) and (b) show the cross-section and the sensor geometry, respectively, while Figure 2 (c) shows the materials of the core and perfectly matched layer (PML) made of silica, the cross-section of the proposed PCF-based SPR sensor. The total number of mesh elements is 158986 and 520 vertices, as shown in Figure 2 (d). The simulation for modal analysis is done in the X-Y plane while the light propagation is along the Z-direction.

3. RESULTS OF DISCUSSIONS

3.1. Simulation of PCF with (Gold/ Silver) and Graphene NPs layer

The PCF sensor model was proposed in this work to utilize surface plasmon resonance for sensing applications; evanescent waves created by light propagation in a fibre may be communicated to the PCF outer surface. The essential parameters for this study are the thickness of Au, Ag, and graphene NPs, the wavelength, and the analyte RIs. The 50 nm thickness of nanolayer coated the PCF sensor was chosen since it provided the highest performance. Then, it was possible to determine the wavelength and the RIs that varied for each liquid and n_{eff}. Then, as it depends on the imaginary part of n_{eff}, Im(n_{eff}) of the fundamental core mode and the wavelength (λ) in nm as in Equation (4) [27-29], the confinement loss (CL) in (dB/m) was measured by:

$$\alpha_{CL} = 8.686 \times \frac{2\pi}{\lambda} \times \mathrm{Im}(n_{\mathrm{eff}}) 10^6 \left(\frac{dB}{m}\right) \quad (4)$$

where Im(n_{eff}) signifies the imaginary part of the effective refractive index, and λ is the operating wavelength.

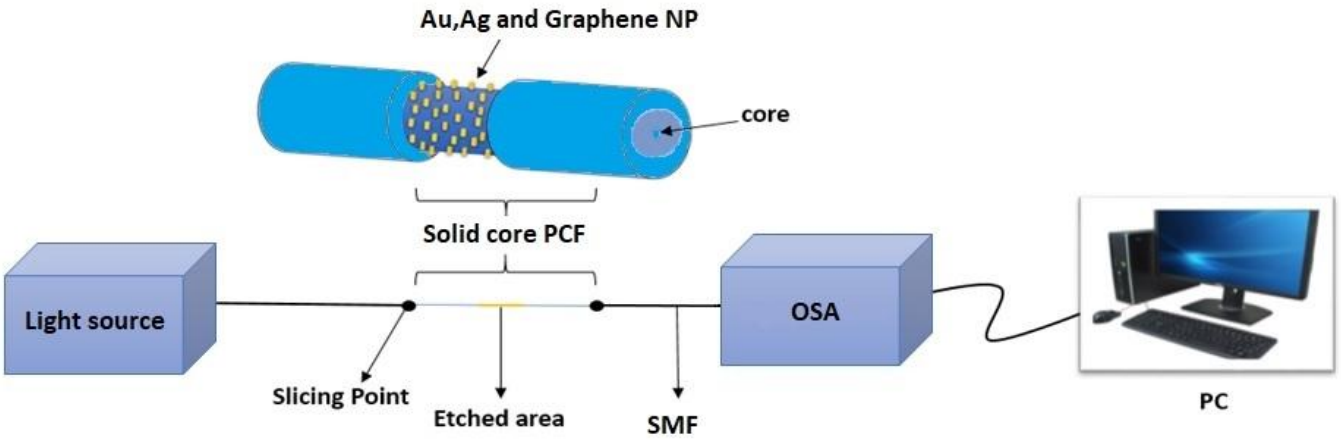

Figure 1. The biosensor arrangement of nanomaterials-based PCF structure

The PCF was created via laser transmission from the fibre core at a wavelength between (1525 and 1560 nm). Using the simulation software COMSOL Multiphysics 6.1, a silica glass core RI resulting from Equation (1) and (gold/silver) layer with a thickness of 50 nm was used to design the PCF hypothetically. The electric field dispersion spectrum of the fundamental mode of glucose is shown in Figure 3 (a) at the confinement loss maximum and core confinement of the electric field. Figures 3 (b) and (c) show the SPR mode. Figures 4 (a) and (b) show the loss spectra calculated from Equation (4) when the analyte RI varies from 1.3475 to 1.3502. The plasmon mode is affected by the RI of the analyte liquid, which changes the phase-matching wavelength between the core and plasmon modes. As the RI of the liquid increases, the resonance wavelength will shift to a longer wavelength direction (Redshift). This is due to a higher effective refractive index (n_{eff}) of the surface plasmon mode modulating the phase matching point. This minimizes the difference between the core-guided and plasmon modes and strengthens the coupling efficiency. The maximum confinement loss was 7.5×10^{-5} and 1.73×10^{-5} at the PCF sensor coated with (Au-graphene and Ag-graphene) nanolayer, respectively. The high loss value refers to increased penetration through the cladding region, indicating the maximum energy transfer from the core-guided mode to the SPR mode. Wavelength sensitivity applying the wavelength and amplitude interrogation method can be determined by Equation (5) [30-32]:

$$S_\lambda = \frac{\Delta\lambda_{peak}}{\Delta na}\,(\mathrm{nm/RIU}) \qquad (5)$$

where $\Delta\lambda_{peak}$ and Δn_a are the difference of wavelength peak shifts and analyte RI variation, respectively.

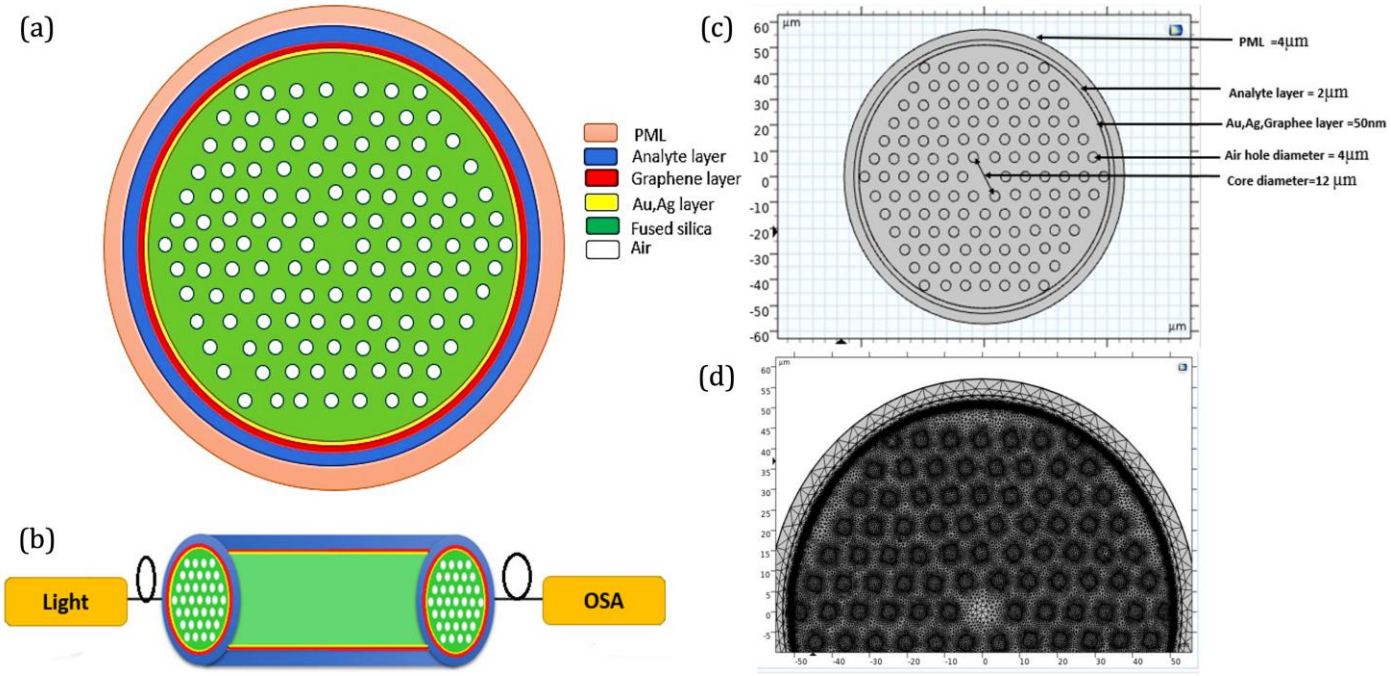

Figure 2. (a) The cross-section structure of the PCF sensor, (b) Geometry of the PCF sensor, (c) The core of PCF, Au-graphene nanolayer, analytic layer, and PML layer, and (d) Mesh of the sensor

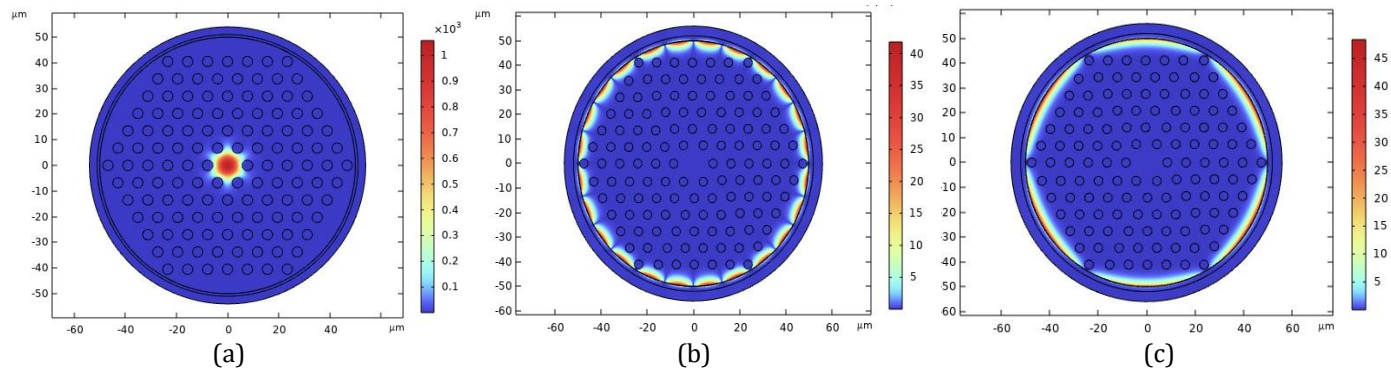

Figure 3. (a) The fundamental mode of PCF. (b) SPR mode of PCF coating by Ag-graphene nanolayer and (c) SPR mode of PCF coating by Au-graphene nanolayer

The proposed sensor has wavelength sensitivity of (4284.243 and 3775.649) nm/RIU for Au-graphene and Ag-graphene coating PCF, respectively, as shown in Figures 5 (a) and (b). The sensor resolution, which describes how the sensor detects a subtle change in the analyte RI, is another important parameter determined by Equation (6) [33-35]:

$$R = \Delta n_a \frac{\Delta\lambda_{peak}}{\Delta\lambda_{min}} (RIU^{-1}) \quad (6)$$

where $\Delta\lambda_{min}$ represents the instrumental peak-wavelength resolution instrumental peak-wavelength resolution and is assumed to be 0.1 μm. We get the highest resolution of 8.33×10^{-6} RIU^{-1} when the analyte's refractive index is varied from 1.3476 to 1.3502 [36, 37].

The developed PCF sensor demonstrates extraordinarily high sensitivity to the liquid analytes, and the large loss peak is triggered at the SPR wavelength. As a result, the SPR

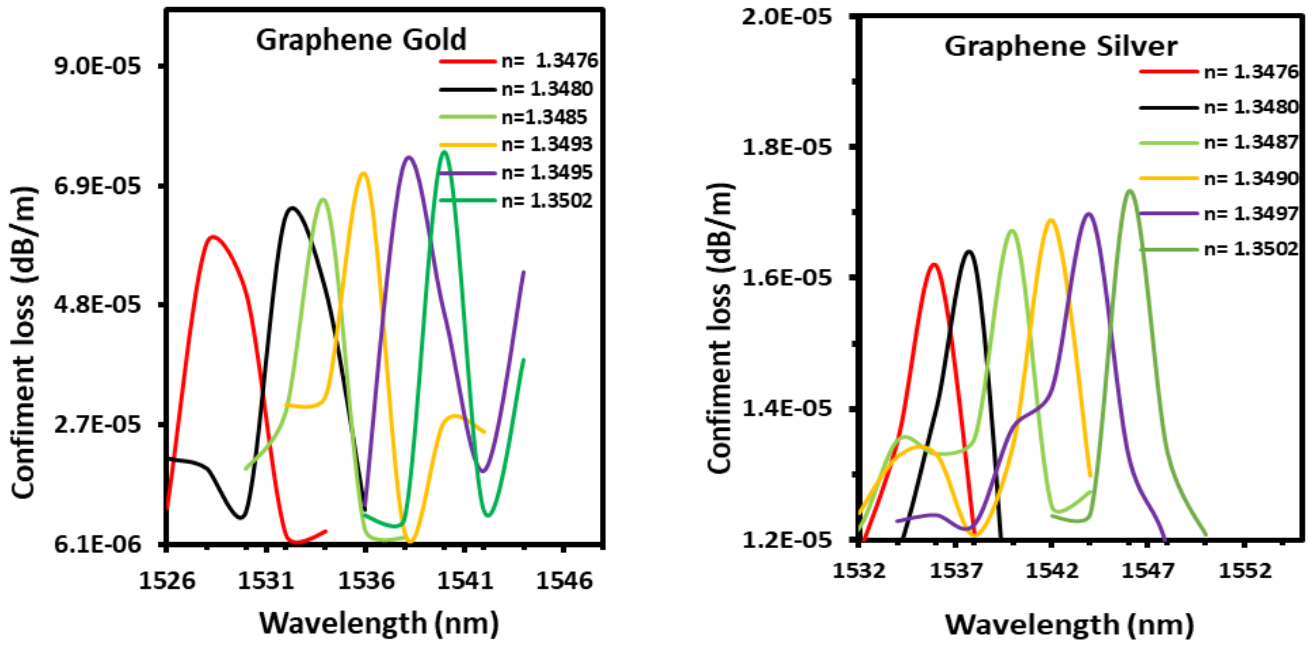

Figure 4. Variation of loss curve with RI of glucose as a function of wavelength (a) PCF coating by Au-graphene nanolayer and (b) PCF coating by Ag-graphene nanolayer

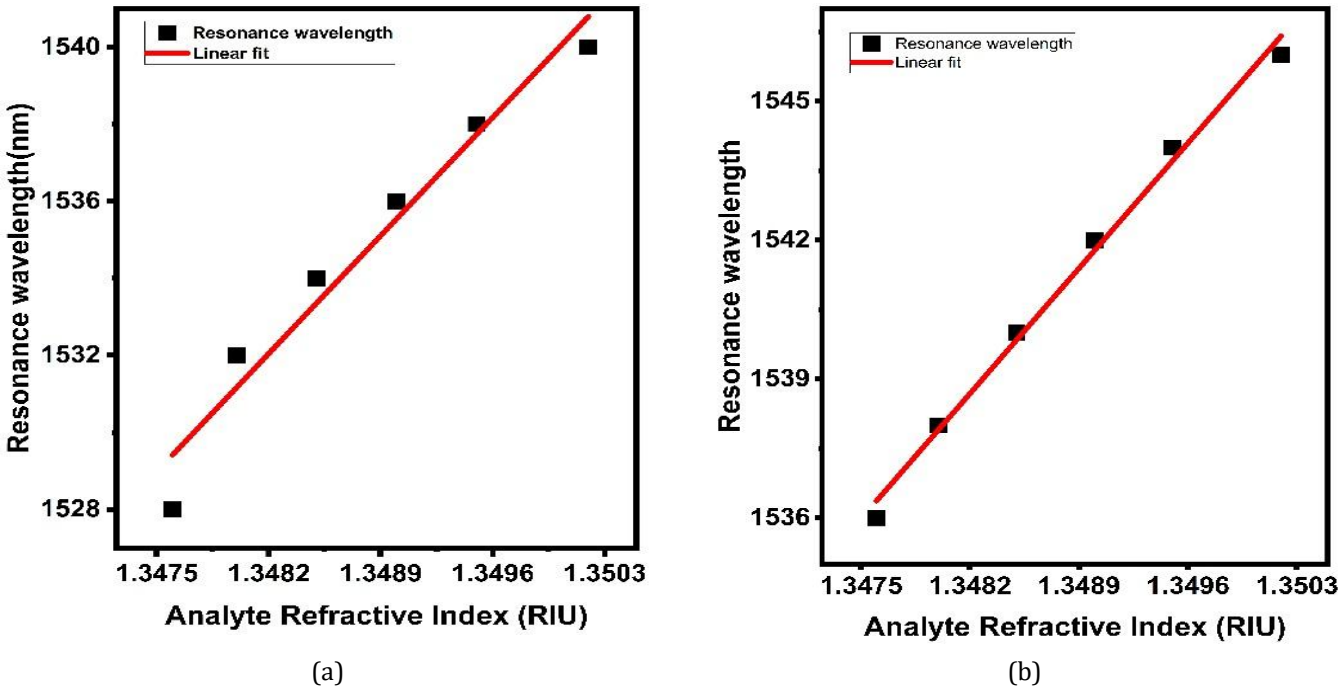

Figure 5. Variation of resonance wavelength with different RI for glucose solution (a) Au-graphene coating PCF and (b) Ag-graphene coating PCF

has been extensively employed in optical fibre detection when the phase match between the core and SPR modes is done in PCF.

3.2. The Experimental Results

3.2.1. Characterization of Graphene

The typical UV-Vis-NIR absorption spectrum of suspensions in the graphene nanostructures shows a plasmonic peak around 300 nm due to n–π* transitions of C=O [3] Figure 6 (a). The FTIR spectrum of the graphene nanostructure was captured between 400 and 4000 cm^{-1}. Figure 6 (b) exhibits the graphene nanostructure FTIR spectra after being created in water. The samples include adsorbed water, as shown by the comparatively large peak at 3411 cm^{-1}, associated with water O—H stretching vibration mode [4]. A peak at 1327 cm^{-1} is attributed to C—H bend in CH_3, whereas a peak at 2936 cm^{-1} is attributed to C—H stretching. Standard infrared spectra reveal that the stretch peak of carbon dioxide is located at 2360 cm^{-1} [46-49]. A band between 1580 and 1450 cm^{-1} is related to the stretching vibration of the hybridized sp^2 c-c bond from the graphene lattice structure [43].

Figure 7 (a) shows manufactured graphene typical transmission electron microscopy (TEM) image [5]. The prepared two-dimensional material appears flat, thin and paper-like in this image. Additionally, the graphene structure can be seen as a single-layer sheet in a few locations and a double-layer sheet in others. As a result of this examination, it can be said that the method employed to manufacture graphene has only one or a few layers [46, 50]. Raman spectra of the graphene are presented in Figure. 7 (b). The main components in the Raman spectra of carbon are the known G and D peaks, which lie at 1200-1450 and 1500-1600 cm^{-1}, respectively, for visible excitation [6]. The D and G peaks can be easily assigned in the "molecular" view of carbon compounds. All polyaromatic hydrocarbons contain these bands. The D band results from the sp2 atoms in the ring breathing modes [7]. The D and G lines, which correspond to the produced graphene, can be seen in the spectra at about 1350 and 1589 cm^{-1}, respectively, in Figure 7 (b).

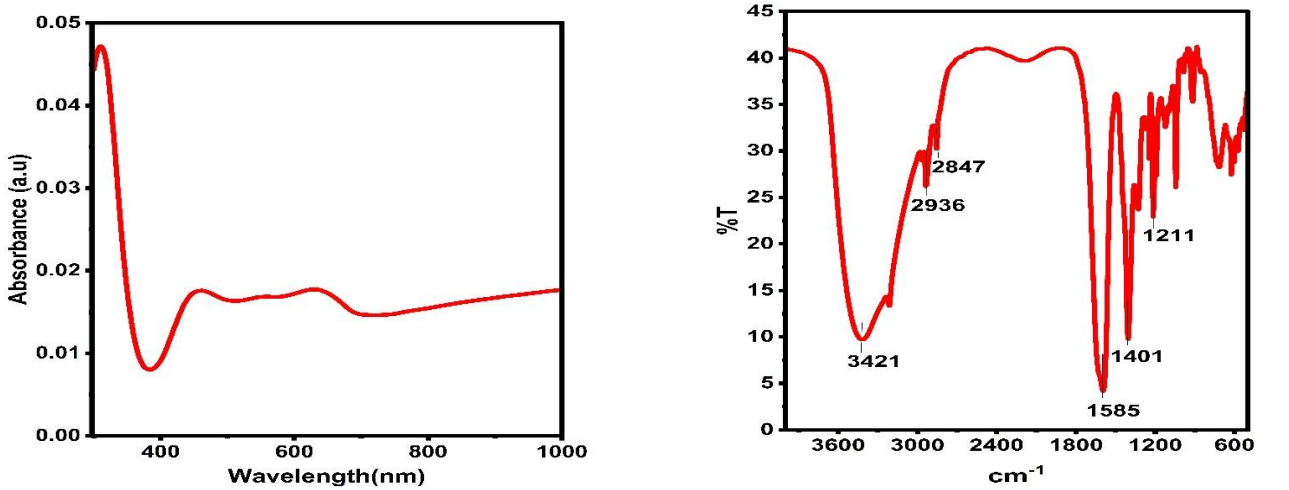

(a) (b)

Figure 6. (a) UV-vis and (b) FT-IR spectrum of graphene nanolayer

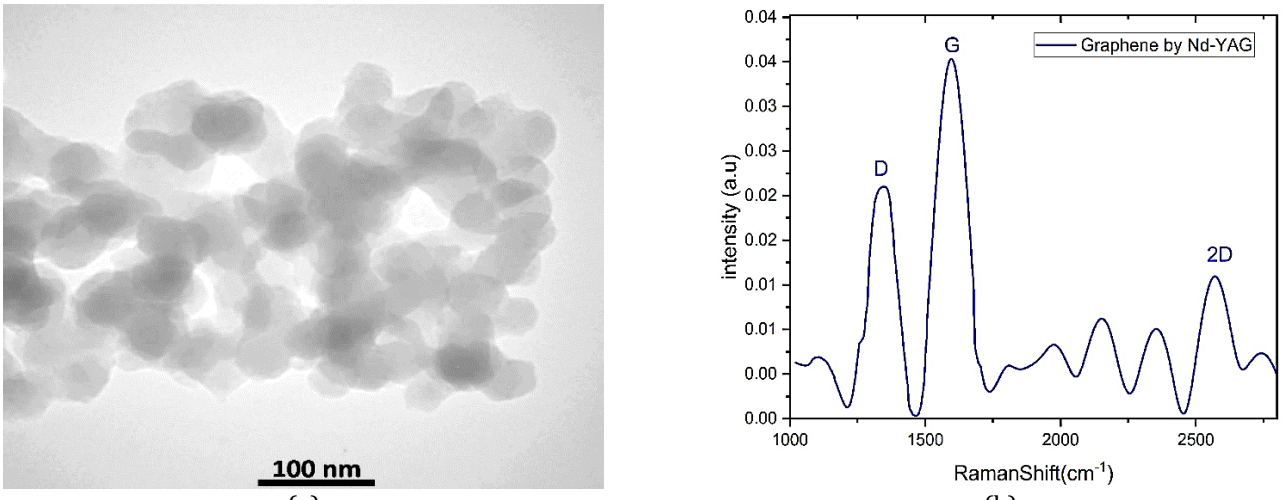

(a) (b)

Figure 7. (a) TEM of graphene nanoparticles and (b) Raman spectra of the graphene nanolayer

The experimental performance of the SPR-PCF sensor can be presented in Figure 8 (a) and (b). The transmission spectrum is computed when the sensor is immersed in the solution using the optical spectrum analyzer. A clear (absorption peak) appears in the transmission spectra due to the electromagnetic field coupling from the core mode to SPR mode near the Au/Ag and graphene nanolayers at the resonant wavelength. The transmission spectrum dip exhibits redshift as the analyte refractive index rises. The matching liquid's refractive index (RI) ranges from 1.3475 to 1.3502.

According to theoretical and experimental observations, the resonance wavelength appears to shift towards the red wavelength. Figure 9 (a) and (b) shows the linear fitting of the resonant wavelength as a function of the analyte RI. It can be concluded that the linear line fitting R2 value is 0.9424, indicating good linearity and its potential applications in practical RI detection. Notable, as the resonance wavelength value increased with an increase in the analyte's refractive index. The experimental results showed that the average sensitivity of the resonance wavelength for PCF coated with Au-graphene is

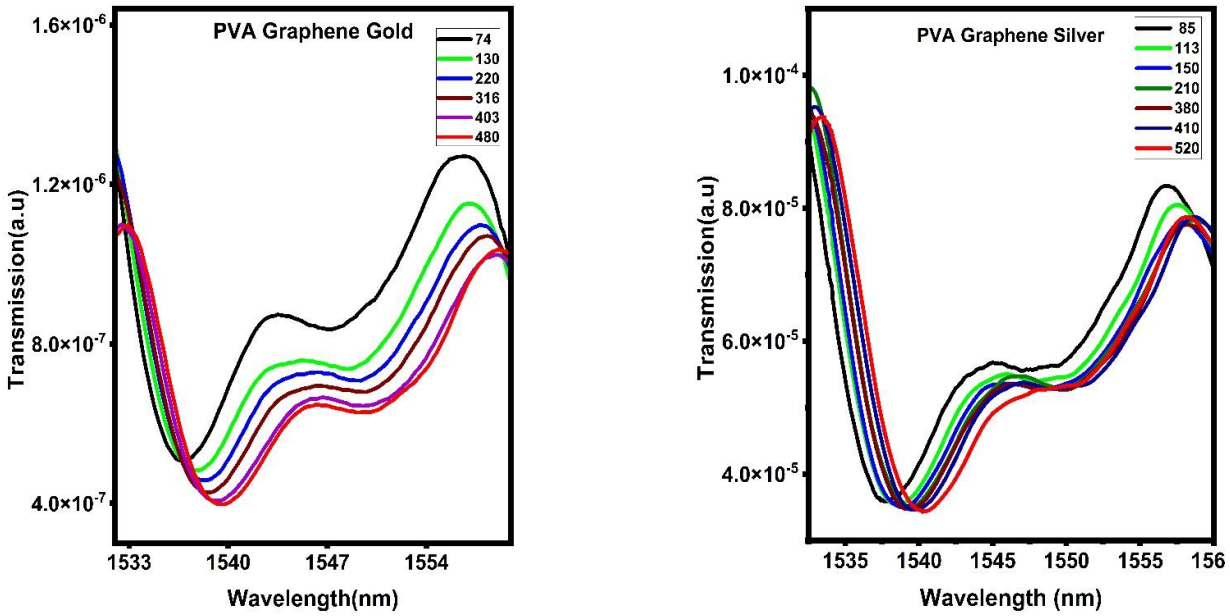

Figure 8. SPR curves of different glucose concentration dissolved blood (a) PCF coating with PVA Au-graphene and (b) PCF coating by PVA Ag-graphene layer

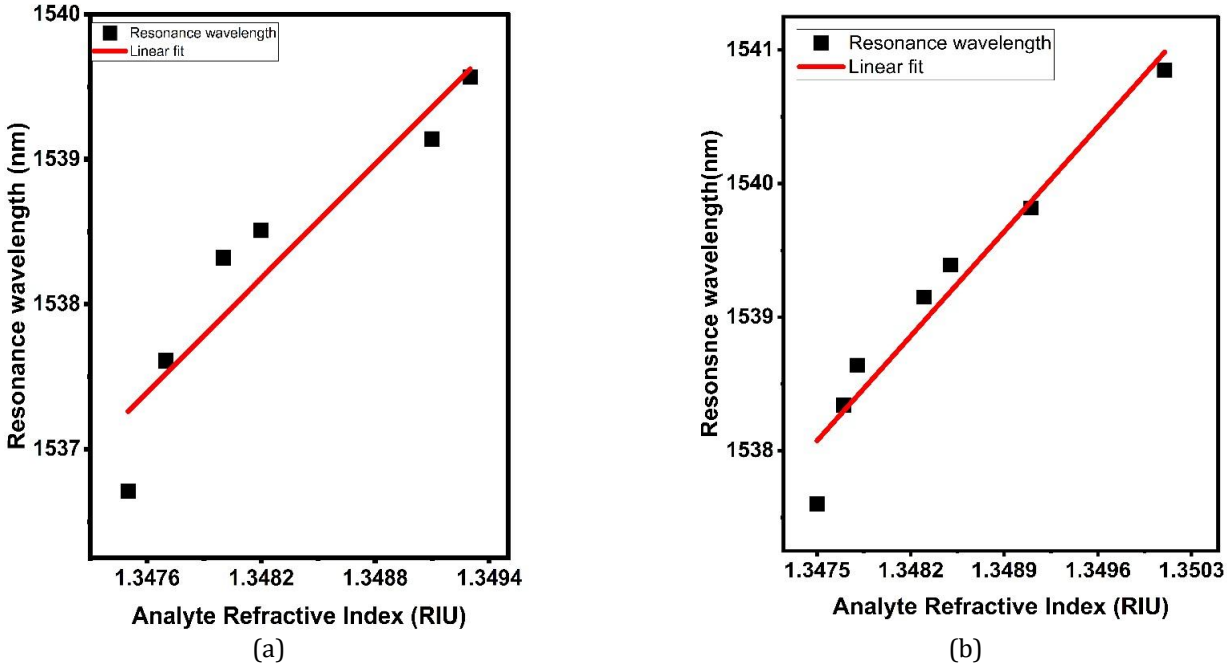

Figure 9. Variation of resonance wavelength with different refractive indices for glucose-dissolved blood at PCF coating with (a) Au-graphene nanolayer and (b) Ag-graphene nanolayer

1314.282 nm/RIU. For PCF coated with Ag-graphene, it is 1119.265 nm/RIU. This is for the analyte refractive index range of 1.3475 to 1.3502.

The Figure of Merit (FOM) of a sensor is the ratio of its sensitivity to the width of its spectral range. A good sensor has a high FOM value, indicating a narrow full width at half maximum (FWHM) of the spectrum and high sensitivity. FOM may also be written as Equation (7) [35]:

$$\text{FOM} = \frac{S_\lambda}{\text{FWHM}} \tag{7}$$

The signal-to-noise ratio (SNR) is an essential measure for determining signal quality in the presence of noise. SNR is an important metric in sensor technology for evaluating the performance of a sensor's ability to differentiate between an intended signal and undesired noise. The signal-to-noise ratio may be calculated using Equation (8) [27]:

$$\text{SNR} = \frac{\Delta\lambda_{\text{peak}}}{\text{FWHM}} \tag{8}$$

The FOM and SNR are shown in Figure 10 (a) and (b) from the simulation result and Figure 11(a) and (b) from the experimental result. The maximum value of the FOM obtained by simulation is 2898.55 and 1867.06 for PCF sensor coating by Au-graphene and Ag-graphene layers, respectively, and the experimental result of FOM is 744.16 and 445.69 for PCF sensor coating by Au-graphene and Ag-graphene layers, respectively. Also, from those figures, the FOM for the glucose sensor shows downward behaviour. The high value of FOM found for PCF is coated with graphene-Au. This is because gold has better plasmonic properties, it interacts more strongly with the analyte, and the materials have unique optical properties. These factors improve the sensor's sensitivity and responsiveness, resulting in more effective detection capability and a higher FOM. The higher FOM value observed in the simulation compared to the experimental result can be attributed to the idealized nature of simulations. Although the photonic crystal fibre (PCF) sensor system has a highly sensitive value. It is subject to different sources of error and uncertainty. Temperature fluctuations, changes in humidity and pressure, and fluctuations in the wavelength of the light source can lead to measurement mistakes, in addition to the efficiency of combining light within and outside PCF, signal noise, sample characteristics, calibration errors, and optical loss could contribute more to uncertainty, respectively. The maximum SNR values for glucose in the blood in simulation are 1.15 and 0.77 for Au-graphene and Ag-graphene coated PCF, and the experimental results were 0.15 and 0.17. A higher resolution of 2.52×10^{-5} and 2.5×10^{-5} for Au-graphene and Ag-graphene nanolayers, respectively.

Figure 12 exhibits the confinement loss for the PCF sensor before and after adding graphene to the gold and silver nanolayers at RI was 1.3502. In this comparison, the loss values increased, and the curve shifted towards longer wavelengths when graphene was added. It is found that when the graphene layer is added to the gold and silver PCF sensor, the sensor sensitivity is remarkably improved. Table 1 gives the sensor parameters (sensitivity, FOM and resolution) with and without the graphene layer.

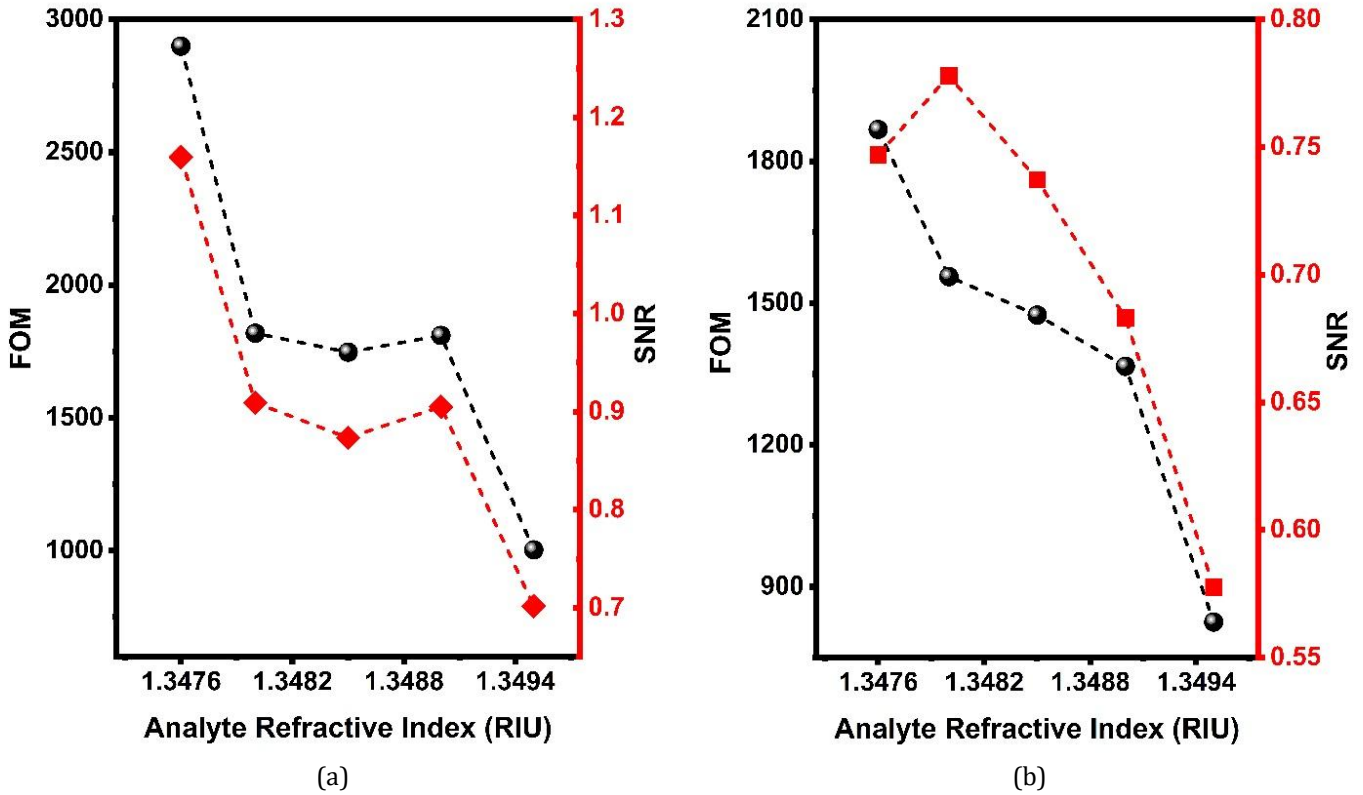

Figure 10. The Figure of Merit and SNR for PCF sensors for (a) Au-graphene and (a) Ag-graphene coating PCF theoretical results

Table 1. The performance parameters for PCF sensor with and without graphene layer

PCF Coating by	Sensitivity (nm/RIU)	FOM	Resolution
Au without graphene	1114.164	321.00	3.34×10^{-5}
Au-graphene	1314.282	744.16	2.50×10^{-5}
Ag without graphene	1012.364	299.00	3.30×10^{-5}
Ag-graphene	1119.265	445.69	2.70×10^{-5}

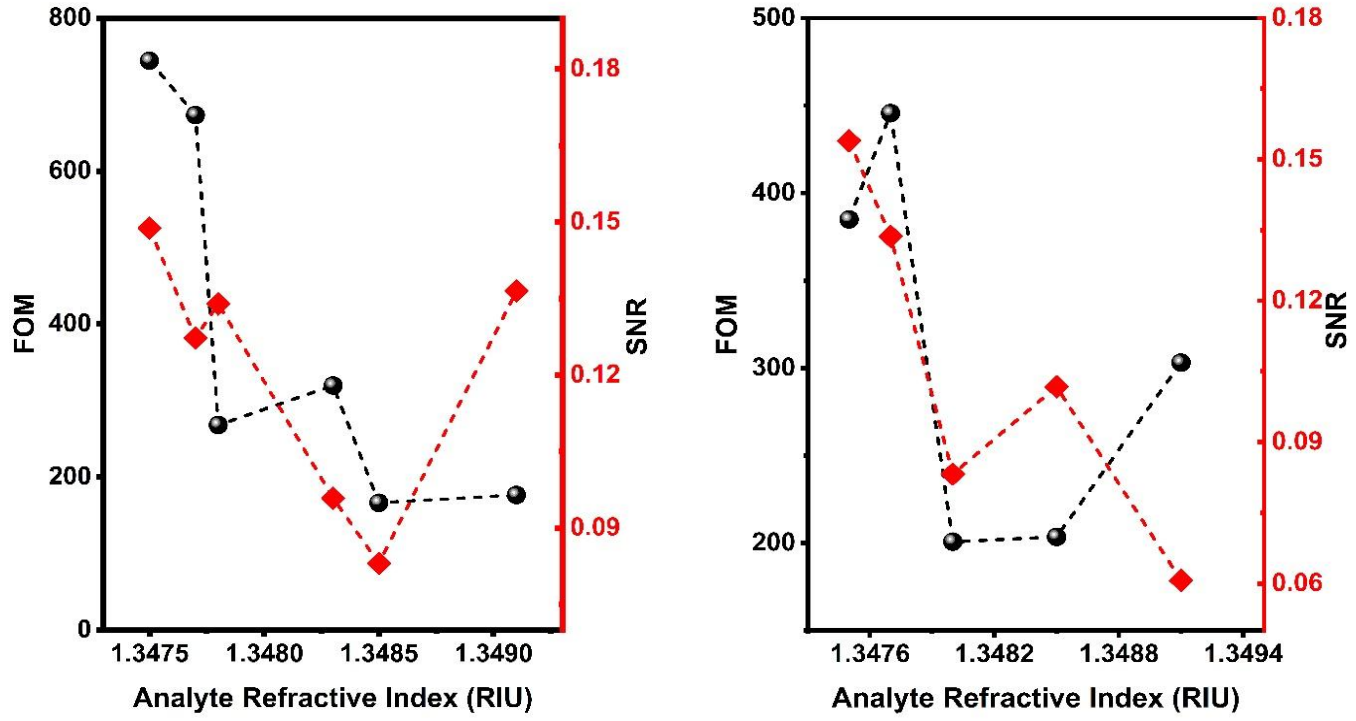

Figure 11. The Figure of Merit and SNR for PCF sensors for (a) Au-graphene and (a) Ag-graphene coating PCF experimental results

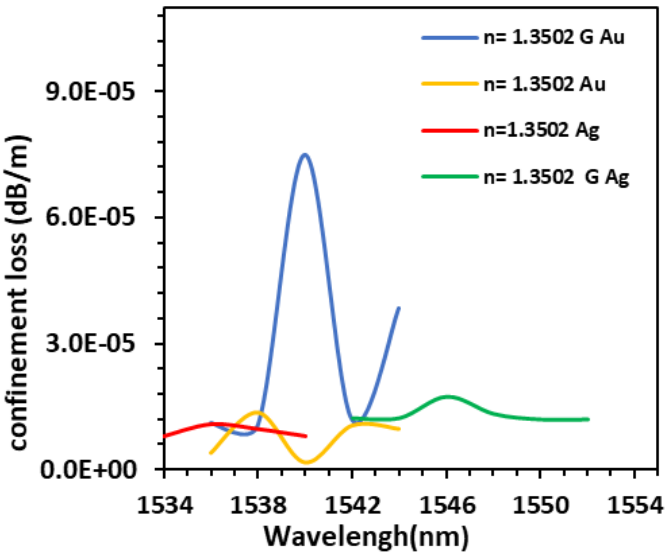

Figure 12. The confinement loss as a function of wavelength for Au and Ag with and without graphene

4. CONCLUSION

In conclusion, the SPR-PCF sensor has been proposed and examined numerically and experimentally. The surface plasmonic resonance PCF sensor with Au-graphene and Ag-graphene nanolayer is presented in this work. Due to the gold/silver and graphene nanolayers on the mid-outer surface of the optical fibre, the manufacturing complexity is reduced. Simple and real-time detection can be done using this sensor by directly immersing the PCF active region into the analyte. The comparison of simulation and experimental results confirms that adding graphene nanoparticles on the outer layer of the gold/silver nanolayer can improve the sensitivity of the PCF sensor. High linearity and a high resolution are achieved. This biosensor could be used in many potential and promising applications in biological and biochemical sensing

REFERENCES

[1] T. Li, L. Zhu, X. Yang, X. Lou, and L. Yu, "A Refractive Index Sensor Based on H-Shaped Photonic Crystal Fibers Coated with Ag-Graphene Layers," *Sensors*, vol. 20, no. 3, p. 741, Jan. 2020, doi: 10.3390/s20030741.

[2] A. A. Rifat, F. haider, R. Ahmed, G. A. Mahdiraji, F. R. Mahamd Adikan, and A. E. Miroshnichenko, "Highly sensitive selectively coated photonic crystal fiber-based plasmonic sensor," *Optics Letters*, vol. 43, no. 4, p. 891, Feb. 2018, doi: 10.1364/OL.43.000891.

[3] D. J. J. Hu and H. P. Ho, "Recent advances in plasmonic photonic crystal fibers: design, fabrication and applications," *Advances in Optics and Photonics*, vol. 9,

no. 2, p. 257, Jun. 2017, doi: 10.1364/AOP.9.000257.

[4] N. H. Jumaah, S. Korkmaz, M. A. Fakhri, and H. J. A. al Bayaty, "Correction: Substrate selection and characterization in infrared detector design for sorting systems," *Journal of Optics*, Jan. 2025, doi: 10.1007/s12596-025-02444-w.

[5] A. A. Rifat, K. Ahmed, S. Asaduzzaman, B. K. Paul, and R. Ahmed, "Development of Photonic Crystal Fiber-Based Gas/Chemical Sensors," in *Computational Photonic Sensors*, Cham: Springer International Publishing, 2019, pp. 287–317. doi: 10.1007/978-3-319-76556-3_12.

[6] M. Mohammed *et al.*, "Fabrication and characterization of zinc oxide nanoparticle-treated kenaf polymer composites for weather resistance based on a solar UV radiation," *BioResources*, vol. 13, no. 3, pp. 6480–6496, Jul. 2018, doi: 10.15376/biores.13.3.6480-6496.

[7] Md. Hasan, S. Akter, A. Rifat, S. Rana, and S. Ali, "A Highly Sensitive Gold-Coated Photonic Crystal Fiber Biosensor Based on Surface Plasmon Resonance," *Photonics*, vol. 4, no. 1, p. 18, Mar. 2017, doi: 10.3390/photonics4010018.

[8] H. Abed, N. Hameed, and E. Salim, "Study of Mechanical and Optical Properties of Nano-hydroxyapatite Dispersed PS/PC Blend Nanocomposites," *International Journal of Nanoelectronics and Materials (IJNeaM)*, vol. 17, no. 1, pp. 117–122, Feb. 2024, doi: 10.58915/ijneam.v17i1.496.

[9] M. F. O. Hameed and S. Obayya, Eds., *Computational Photonic Sensors*. Cham: Springer International Publishing, 2019. doi: 10.1007/978-3-319-76556-3.

[10] Z. H. Tawfiq, M. A. Fakhri, and S. A. Adnan, "Photonic Crystal Fibres PCF for Different Sensors in Review," *IOP Conference Series: Materials Science and Engineering*, vol. 454, p. 012173, Dec. 2018, doi: 10.1088/1757-899X/454/1/012173.

[11] C. Liu *et al.*, "Surface plasmon resonance (SPR) infrared sensor based on D-shape photonic crystal fibers with ITO coatings," *Optics Communications*, vol. 464, p. 125496, Jun. 2020, doi: 10.1016/j.optcom.2020.125496.

[12] E. Y. Salih, "Opto-electrical evaluation of visible blind fast-response nanostructured SnO_2/Si photodetector," *RSC Advances*, vol. 14, no. 38, pp. 27733–27740, 2024, doi: 10.1039/D4RA05303F.

[13] W. L. Ng, A. A. Rifat, W. R. Wong, G. A. Mahdiraji, and F. R. Mahamd Adikan, "A Novel Diamond Ring Fiber-Based Surface Plasmon Resonance Sensor," *Plasmonics*, vol. 13, no. 4, pp. 1165–1170, Aug. 2018, doi: 10.1007/s11468-017-0617-y.

[14] Evan T. Salim, Ahmed T. Hassan, Rana O Mahdi, and Forat H. Alsultany, "Physical Properties of HfO_2 Nano Structures Deposited using PLD," *International Journal of Nanoelectronics and Materials (IJNeaM)*, vol. 16, no. 3, pp. 495–510, Oct. 2024, doi: 10.58915/ijneam.v16i3.1266.

[15] Q. Liu, Z. Ma, Q. Wu, and W. Wang, "The biochemical sensor based on liquid-core photonic crystal fiber filled with gold, silver and aluminum," *Optics & Laser Technology*, vol. 130, p. 106363, Oct. 2020, doi: 10.1016/j.optlastec.2020.106363.

[16] E. T. Salim, J. A. Saimon, M. K. Abood, and F. H. Alsultany, "A Preliminary Study on Structural and Optical Properties of Heat Treated Nb_2O_5 Nanostructure," *International Journal of Nanoelectronics and Materials (IJNeaM)*, vol. 16, no. 1, pp. 21–32, Oct. 2024, doi: 10.58915/ijneam.v16i1.910.

[17] A. A. Rifat *et al.*, "Copper-Graphene-Based Photonic Crystal Fiber Plasmonic Biosensor," *IEEE Photonics Journal*, vol. 8, no. 1, pp. 1–8, Feb. 2016, doi: 10.1109/JPHOT.2015.2510632.

[18] M. K. Abood, M. H. A. Wahid, J. A. Saimon, and E. T. Salim, "Physical Properties of Nb_2O_5 Thin Films Prepared at 12M Ammonium Concentration," *International Journal of Nanoelectronics and Materials (IJNEAM)*, vol. 11 (Special Issue), pp. 237–244, Dec. 2018.

[19] J. N. Dash and R. Jha, "Graphene-Based Birefringent Photonic Crystal Fiber Sensor Using Surface Plasmon Resonance," *IEEE Photonics Technology Letters*, vol. 26, no. 11, pp. 1092–1095, Jun. 2014, doi: 10.1109/LPT.2014.2315233.

[20] A. Y. kudhur, E. T. Salim, I. Kara, R. O. Mahdi, and R. K. Ibrahim, "The effect of laser energy on Cu_2O nanoparticles formation by liquid-phase pulsed laser ablation," *Journal of Optics*, vol. 53, no. 2, pp. 1309–1321, Apr. 2024, doi: 10.1007/s12596-023-01319-2.

[21] V. Kaur and S. Singh, "Design of titanium nitride coated PCF-SPR sensor for liquid sensing applications," *Optical Fiber Technology*, vol. 48, pp. 159–164, Mar. 2019, doi: 10.1016/j.yofte.2018.12.015.

[22] E. K. Akowuah, T. Gorman, H. Ademgil, S. Haxha, G. K. Robinson, and J. V. Oliver, "Numerical Analysis of a Photonic Crystal Fiber for Biosensing Applications," *IEEE Journal of Quantum Electronics*, vol. 48, no. 11, pp. 1403–1410, Nov. 2012, doi: 10.1109/JQE.2012.2213803.

[23] M. S. A. Gandhi, P. R. Babu, K. Senthilnathan, and Q. Li, "High sensitivity photonic crystal fiber-based refractive index microbiosensor," *Optical Fiber Technology*, vol. 46, pp. 88–94, Dec. 2018, doi: 10.1016/j.yofte.2018.09.016.

[24] R. A. Abbas, E. T. Salim, and R. O. Mahdi, "Morphology transformation of Cu_2O thin film: different environmental temperatures employing chemical method," *Journal of Materials Science: Materials in Electronics*, vol. 35, no. 16, p. 1057, Jun. 2024, doi: 10.1007/s10854-024-12823-x.

[25] E. Yahya Salih, "Fabrication of CdSe/Si nanostructure for self-powered visible light photodetector," *Materials Letters*, vol. 371, p. 136930, Sep. 2024, doi: 10.1016/j.matlet.2024.136930.

[26] M. S. Muhsin, E. T. Salim, and J. A. Saimon, "Structural, morphological and optical properties of tungsten trioxide nanoparticle synthesis by pulsed laser ablation in water: effect of laser fluence," *Journal of Optics*, vol. 53, no. 3, pp. 2339–2354, Jul. 2024, doi: 10.1007/s12596-023-01368-7.

[27] L. Shahriary, H. Ghourchian, and A. A. Athawale, "Graphene-Multiwalled Carbon Nanotube Hybrids Synthesized by Gamma Radiations: Application as a Glucose Sensor," *Journal of Nanotechnology*, vol. 2014, pp. 1–10, 2014, doi: 10.1155/2014/903872.

[28] H. S. Ali and M. A. Fakhri, "An Overview of Au Photonic Crystal Fiber of Sensors," *Materials Science Forum*, vol. 1002, pp. 282–289, Jul. 2020, doi: 10.4028/www.scientific.net/MSF.1002.282.

[29] K. Krishnamoorthy, G.-S. Kim, and S. J. Kim, "Graphene nanosheets: Ultrasound assisted synthesis and characterization," *Ultrasonics Sonochemistry*, vol. 20, no. 2, pp. 644–649, Mar. 2013, doi: 10.1016/j.ultsonch.2012.09.007.

[30] S. Osamah, A. A. Alwahib, and M. A. Fakhri, "D-shape optical fibers based on gold nanoparticles for a different sensors: A review," 2022, p. 020135. doi: 10.1063/5.0107768.

[31] Z. Çiplak, N. Yildiz, and A. Çalimli, "Investigation of Graphene/Ag Nanocomposites Synthesis Parameters for Two Different Synthesis Methods," *Fullerenes, Nanotubes and Carbon Nanostructures*, vol. 23, no. 4, pp. 361–370, Apr. 2015, doi: 10.1080/1536383X.2014.894025.

[32] M. T. Awayiz and E. T. Salim, "Photo Voltaic Properties of Ag_2O/ Si Heterojunction Device: Effect of Substrate Conductivity," *Materials Science Forum*, vol. 1002, pp. 200–210, Jul. 2020, doi: 10.4028/www.scientific.net/MSF.1002.200.

[33] M. Hayyan, A. Abo-Hamad, M. A. AlSaadi, and M. A. Hashim, "Functionalization of graphene using deep eutectic solvents," *Nanoscale Research Letters*, vol. 10, no. 1, p. 324, Dec. 2015, doi: 10.1186/s11671-015-1004-2.

[34] S. Kamali, E. Solati, and D. Dorranian, "Effect of Laser Fluence on the Characteristics of Graphene Nanosheets Produced by Pulsed Laser Ablation in Water," *Journal of Applied Spectroscopy*, vol. 86, no. 2, pp. 238–243, May 2019, doi: 10.1007/s10812-019-00806-4.

[35] N. K. Hassan, M. A. Fakhri, E. T. Salim, and M. A. Hassan, "Gold nano particles based optical fibers for a different sensor in a review," *Materials Today: Proceedings*, vol. 42, pp. 2769–2772, 2021, doi: 10.1016/j.matpr.2020.12.719.

[36] R. A. Abbas, E. T. Salim, and R. O. Mahdi, "Deposition time effect on copper oxide nano structures, an analysis study using chemical method," *Journal of Materials Science: Materials in Electronics*, vol. 35, no. 6, p. 427, Feb. 2024, doi: 10.1007/s10854-024-12143-0.

[37] H. S. Ali, M. A. Fakhri, and Z. Khalifa, "Optical and Structural Properties of the Gold Nanoparticles Ablated by Laser Ablation in Ethanol for Biosensors," *Journal of Physics: Conference Series*, vol. 1795, no. 1, p. 012065, Mar. 2021, doi: 10.1088/1742-6596/1795/1/012065.

[38] E. Salim, R. Fadhil, and W. Kalif, "Synthesis of $LiNbO_3$ microstructures: structural, optical, and surface morphology using Chemical bath deposition (CBD) method without post-heat treatment," *Egyptian Journal of Chemistry*, vol. 66, no. 4, pp. 63–70, Jul. 2022, doi: 10.21608/ejchem.2022.129669.5749.

[39] A. D. Faisal, W. K. Khalef, E. T. Salim, F. H. Alsultany, and M. H. A. Wahid, "Conductivity Modification of ZnO NRs Films via Gold Coating for Temperature Sensor Application," *Key Engineering Materials*, vol. 936, pp. 105–114, Dec. 2022, doi: 10.4028/p-25h5n1.

[40] S. Preussler, H. Al-Taiy, and T. Schneider, "Generation and Stabilization of THz-waves with Extraordinary Low Line Width and Phase Noise," in *CLEO: 2015*, Washington, D.C.: OSA, 2015, p. STu4H.6. doi: 10.1364/CLEO_SI.2015.STu4H.6.

[41] M. S. Alwazny, R. A. Ismail, and Evan. T. Salim, "Aggregation threshold for Novel Au – $LiNbO_3$ core/shell Nano composite: effect of laser ablation energy fluence," *International Journal of Nanoelectronics and Materials (IJNEAM)*, vol. 15, no. 3, pp. 223–232, Jul. 2022.

[42] S. M. Tariq, M. A. Fakhri, E. T. Salim, U. Hashim, and F. H. Alsultany, "Design of an unclad single-mode fiber-optic biosensor based on localized surface plasmon resonance by using COMSOL Multiphysics 5.1 finite element method," *Applied Optics*, vol. 61, no. 21, p. 6257, Jul. 2022, doi: 10.1364/AO.458175.

[43] E. T. Salim, A. A. Taha, S. A. Abdullatef, and M. M. Farhan, "Anti-microbial and anti-tumor activity of niobium oxide nano powder," *AIP Conference Proceedings*, vol. 2400, no. 1, p. 030015, Oct. 2022, doi: 10.1063/5.011213.

[44] A. L. Abed, W. K. Khalef, and E. T. Salim, "Synthesis, Characterization and Optoelectronic device application of ZnO nano structure," *Journal of Physics: Conference Series*, vol. 1795, no. 1, p. 012031, Mar. 2021, doi: 10.1088/1742-6596/1795/1/012031.

[45] M. S. Alwazny, R. A. Ismail, and E. T. Salim, "High-quantum efficiency of Au@$LiNbO_3$ core–shell nano composite as a photodetector by two-step laser ablation in liquid," *Applied Physics A*, vol. 128, no. 6, p. 500, Jun. 2022, doi: 10.1007/s00339-022-05651-5.

[46] S. M. Tariq and M. A. Fakhri, "Design and Simulation of Optical Fibre Based of Gold Nanoparticles for Sensor Applications," *International Journal of Nanoelectronics and Materials (IJNEAM)*, vol. 15 (Special Issue), pp. 59–70, Dec. 2022.

[47] A. M. Yahya, A. I. Hassan, E. T. Salim, and A. J. Addie, "Hybrid nanocomposites for enhanced photodetection: Synthesis and application of Ag_2O@Graphene/Si heterojunctions," *Journal of Alloys and Compounds*, vol. 1001, p. 175133, Oct. 2024, doi: 10.1016/j.jallcom.2024.175133.

[48] M. M. Salih, "Water Pollution Detection of Tigris River by Utilizing Thermal Remote Sensing Techniques: North Baghdad-Iraq Region as a Case Study," *Optica Pura y Aplicada*, vol. 54, no. 1, pp. 1–9, Mar. 2021, doi: 10.7149/OPA.54.1.51045.

[49] R. A. Ismail, E. T. Salim, and M. S. Alwazny, "Nanosecond Laser Ablation of Au@$LiNbO_3$ Core–Shell Nanoparticles in Ethanol: Properties and Application in Optoelectronic Devices," *Plasmonics*, vol. 18, no. 2, pp. 561–576, Apr. 2023, doi: 10.1007/s11468-022-01780-y.

[50] M. A. Fakhri *et al.*, "A gold nanoparticles coated unclad single mode fiber-optic sensor based on localized

surface plasmon resonance," *Scientific Reports*, vol. 13, no. 1, p. 5680, Apr. 2023, doi: 10.1038/s41598-023-32852-6.